Liquid Crystals
Publication details, including instructions for authors and subscription information:
http://www.informaworld.com/smpp/title~content=t713926090

Symmetric liquid crystal dimers containing hydrazide groups: parity-dependent smectic structure, hydrogen bonding and substitution effect

Haitao Wang[ab]; Renfan Shao[b]; Chenhui Zhu[b]; Binglian Bai[a]; Chengbo Gong[a]; Peng Zhang[a]; Fan Li[a]; Min Li[a]; Noel A. Clark[b]
[a] Key Laboratory of Automobile Materials (MOE) & College of Materials Science and Engineering, Jilin University, Changchun 130012, People's Republic of China [b] Department of Physics, University of Colorado, Boulder, CO 80309, USA

To cite this Article Wang, Haitao , Shao, Renfan , Zhu, Chenhui , Bai, Binglian , Gong, Chengbo , Zhang, Peng , Li, Fan , Li, Min and Clark, Noel A.(2008) 'Symmetric liquid crystal dimers containing hydrazide groups: parity-dependent smectic structure, hydrogen bonding and substitution effect', Liquid Crystals, 35: 8, 967 — 974
To link to this Article: DOI: 10.1080/02678290802308035
URL: http://dx.doi.org/10.1080/02678290802308035

Liquid Crystals,
Vol. 35, No. 8, August 2008, 967–974

Taylor & Francis
Taylor & Francis Group

Symmetric liquid crystal dimers containing hydrazide groups: parity-dependent smectic structure, hydrogen bonding and substitution effect

Haitao Wang[ab], Renfan Shao[b], Chenhui Zhu[b], Binglian Bai[a], Chengbo Gong[a], Peng Zhang[a], Fan Li[a], Min Li[a]* and Noel A. Clark[b]

[a]*Key Laboratory of Automobile Materials (MOE) & College of Materials Science and Engineering, Jilin University, Changchun 130012, People's Republic of China;* [b]*Department of Physics, University of Colorado, Boulder, CO 80309, USA*

(Received 13 March 2008; final form 27 June 2008)

Dimeric hydrazide derivatives with long terminal alkoxy chains, i.e. α,ω-bis[*N*-(4-hexadecyloxybenzoyl)-*N*′-(benzoyl-4′-oxy)hydrazine]alkanes (**C16.*n*.C16**, C16 indicates the terminal hexadecyloxy chain; $n=3$, 5, 6, 10, indicates the number of the carbon atoms in the spacer) were synthesised. The liquid crystalline properties were investigated by differential scanning calorimetry, polarising optical microscopy and X-ray diffraction. The dimers with shorter spacer (**C16.*n*.C16**, $n=3$, 5, 6) exhibit enantiotropic smectic phases, whereas **C16.10.C16** with the longest spacer is non-mesomorphic. Furthermore, the smectic structure is parity dependent, i.e. **C16.3.C16** and **C16.5.C16** with odd spacer exhibit a monolayer smectic A phase, whereas **C16.6.C16** with even spacer exhibits a monolayer smectic C phase, in which the incompatibility between the terminal chains, mesogenic groups and the spacers is considered to be the driving force. The results are compared with those for the terminally nitro-substituted series, α,ω-bis[*N*-(4-nitrobenzoyl)-*N*′-(benzoyl-4′-oxy)hydrazine]alkanes (**N*n***), which exhibit an intercalated smectic A phase. Temperature-dependent IR spectroscopic analysis on these two kind of dimers suggests that intermolecular hydrogen bonding, as well as the dipole–dipole interaction arising from the strong polar substituents ($-NO_2$) synergistically drives the intercalated structure of **N*n***. Although hydrogen bonding exists in the monolayer smectic phase of **C16.*n*.C16**, microphase segregation is in favour of the monolayer smectic structure, preventing the formation of an intercalated structure.

Keywords: liquid crystal dimers; intercalated smectic phase; hydrazide derivatives; hydrogen bonding; bent-shaped molecule; smectic A phase; smectic C phase

1. Introduction

Liquid crystal dimers are composed of molecules containing two mesogenic groups linked via a flexible spacer (*1–4*). Although their first discovery dates back to Vorländer (*5*), it was not until many years later that they were recognised as model compounds of semi-flexible main-chain liquid crystal polymers (*6*); such compounds have become a subject of considerable interest. Recently, due to their novel molecular architecture [linear (*5–7*), H-shaped (*8*), T-shaped (*9*), etc.], unique phase behaviours (especially the odd–even effect) and mesophase polymorphism [e.g. biaxial nematic (*10*), intercalated smectic (*11–13*) and columnar B_1 phase (*14*), liquid crystal dimers have attracted much attention in their own right (*1–4*).

Dimers containing identical mesogenic units are referred to as symmetric dimers, whereas those that consist of two differing mesogenic groups are non-symmetric dimers. As has been reported, symmetric dimers containing terminal alkyl chains appear to have a strong tendency to exhibit monolayer smectic phases, the driving force for which is thought to be the incompatibility between the terminal alkyl chains and the spacers, leading to a microphase separation into three regions: terminal chains, mesogenic groups and flexible alkyl spacers (*11, 15*).

In contrast, non-symmetric liquid crystal dimers usually exhibit intercalated smectic phases, in which specific intermolecular interactions between the two different mesogenic units are responsible for this specific phase behaviour (*11*). The question arose, what would happen if the interaction between the identical mesogenic units in the symmetric dimers increases? To answer this question, we have designed a series of symmetric liquid crystal dimers bearing a hydrazide group as the mesogenic units (see Scheme 1), in which the lateral intermolecular hydrogen bonding is expected to increase the intermolecular interaction.

In our previous work, it has been demonstrated that symmetric liquid crystal dimers, α,ω-bis[*N*-(4-nitrobenzoyl)-*N*′-(benzoyl-4′-oxy)hydrazine]alkanes (see Scheme 1, **N*n***, *n* indicates the number of the carbon atoms in the spacer), exhibit an intercalated smectic A phase (SmA_c), for which intermolecular hydrogen bonding between hydrazide groups and the dipole–dipole interaction arising from the nitro

*Corresponding author. Email: minli@mail.jlu.edu.cn

ISSN 0267-8292 print/ISSN 1366-5855 online

DOI: 10.1080/02678290802308035
http://www.informaworld.com

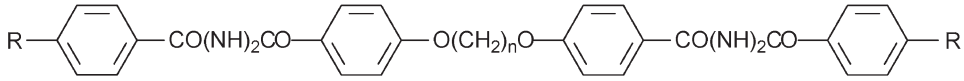

N*n*: R = -NO_2, *n* = 5, 6, 10 ; M6: R=-CH_3, *n*=6; C16.*n*.C16: R=-$OC_{16}H_{33}$, *n* = 3, 5, 6, 10

Scheme 1. The molecular structures of **N*n***, **M6** and **C16.*n*.C16**.

substitution are considered to be the driving forces (*13*). However, in that instance, the interaction between terminal alkoxy chain and the spacer was omitted. So, in order to investigate this interaction, we have prepared symmetric dimers with long terminal alkoxy chains, i.e. α,ω-bis[*N*-(4-hexadecyloxybenzoyl)-*N*′-(benzoyl-4′-oxy)hydrazine] alkanes (**C16.*n*.C16**, C16 indicates the terminal hexadecyloxy chain; *n*=3, 5, 6, 10, indicate the number of the carbon atoms in the spacer, see Scheme 1). The present work will deal with the phase behaviours and mesophase structures of **C16.*n*.C16**, and these results will be further compared with those for **N*n*** (Scheme 1).

2. Experimental

Synthesis

C16.*n*.C16 (*n*=3, 5, 6, 10) were synthesised through a route similar to that for **N*n*** (*13*). The synthesis of the intermediates was according to literature methods (*16, 17*), and the target compounds were obtained through the reaction of α,ω-bis(4-hydrazinylbenzoyl-1-oxy)alkane with 4-hexadecyloxybenzoyl chloride (mole ratio=1:2) in tetrahydrofuran at room temperature. A small amount of pyridine as catalyst was added to the reaction mixtures. All the resulting compounds were purified through repeated recrystallisation from DMSO for further ^{1}H NMR measurements and elemental analysis. Yields were more than 80%.

*1,3-bis[N-(4-cetyloxybenzoyl)-N′-(benzoyl-4′-oxy)-hydrazine]propane (**C16.3.C16**).*

^{1}H NMR (500 MHz, DMSO): δ 10.26 (s, 2H), 10.25 (s, 2H), 7.90 (d, 4H, *J*=8.8 Hz), 7.88 (d, 4H, *J*=8.8 Hz), 7.08 (d, 4H, *J*=8.7 Hz), 7.02 (d, 4H, *J*=8.8 Hz), 4.24 (t, 4H, *J*=6.1 Hz), 4.04 (t, 4H, *J*=6.5 Hz), 2.24 (m, 2H), 1.73 (m, 4H), 1.41 (m, 4H), 1.24 (s, 48H), 0.85 (t, 6H, *J*=6.8 Hz). FT-IR (KBr disc, cm^{-1}): 3227, 2851, 1604, 1570, 1505, 1461, 1308, 1250, 1178, 1112, 1017, 845, 751, 662, 617. Elemental analysis: calculated for $C_{63}H_{92}N_4O_8$, C 73.22, H 8.97, N 5.42; found, C 72.99, H 8.92, N 5.22%.

*1,5-bis[N-(4-cetyloxybenzoyl)-N′-(benzoyl-4′-oxy)-hydrazine]pentane (**C16.5.C16**).*

^{1}H NMR (500 MHz, DMSO): δ 10.26 (s, 4H), 7.89 (d, 4H, *J*=8.6 Hz), 7.88 (d, 4H, *J*=8.6 Hz), 7.04 (d, 4H, *J*=9.0 Hz), 7.02 (d, 4H, *J*=8.9 Hz), 4.09 (t, 4H, *J*=6.3 Hz), 4.03 (t, 4H, *J*=6.5 Hz), 1.83 (m, 4H), 1.73 (m, 4H), 1.60 (m, 2H), 1.41 (m, 4H), 1.24 (s, 48H), 0.85 (t, 6H, *J*=6.8 Hz). FT-IR (KBr disc, cm^{-1}): 3225, 2919, 2851, 1600, 1519, 1460, 1250, 1177, 1113, 1027, 843, 750, 718, 658, 619, 495. Elemental analysis: calculated for $C_{65}H_{96}N_4O_8$, C 73.55, H 9.12, N 5.28; found, C 73.50, H 9.20;, N 5.27%.

*1,6-bis[N-(4-cetyloxybenzoyl)-N′-(benzoyl-4′-oxy)-hydrazine]hexane (**C16.6.C16**).*

^{1}H NMR (500 MHz, DMSO): δ 10.26 (s, 4H), 7.89 (d, 8H, *J*=6.2 Hz), 7.04 (m, 8H), 4.06 (m, 8H), 1.75 (m, 8H), 1.51 (m, 4H), 1.42 (m, 4H), 1.25 (s, 48H), 0.86 (t, 6H, *J*=6.3 Hz). FT-IR (KBr disc, cm^{-1}): 3218, 2921, 2851, 1602, 1568, 1518, 1456, 1395, 1309, 1252, 1176, 1111, 1025, 842, 801, 753, 720, 693, 658, 623, 549, 495. Elemental analysis: calculated for $C_{66}H_{98}N_4O_8$, C 73.71, H 9.18, N 5.21; found, C 73.65, H 9.24, N 4.93%.

*1,10-bis[N-(4-cetyloxybenzoyl)-N′-(benzoyl-4′-oxy)-hydrazine]decane (**C16.10.C16**).*

^{1}H NMR (500 MHz, DMSO): δ 10.25 (s, 4H), 7.88 (d, 8H, *J*=8.1 Hz), 7.03 (d, 4H, *J*=8.7 Hz), 7.02 (d, 4H, *J*=8.7 Hz), 4.04 (m, 8H), 1.72 (m, 8H), 1.41 (m, 8H), 1.32 (s, 8H), 1.24 (s, 48H), 0.85 (t, 6H, *J*=6.8 Hz). FT-IR (KBr disc, cm^{-1}): 3228–2920, 2851, 1608, 1568, 1504, 1459, 1413, 1393, 1308, 1231, 1175, 1110, 1046, 1019, 841, 752, 720, 693, 657, 618, 545, 493. Elemental analysis: calculated for $C_{70}H_{106}N_4O_8$, C 74.30, H 9.44, N 4.95; found, C 74.15, H 9.51, N 4.61%.

Characterisation

^{1}H NMR spectra were recorded with a Bruker Avance 500′MHz spectrometer, using DMSO-d_6 as solvent and tetramethylsilane as an internal standard. FT-IR spectra at room temperature were recorded with a Perkin-Elmer spectrometer (Spectrum One B),

whereas temperature-dependent FT-IR spectra were recorded with a Nicolet Nexus 670 spectrometer. Phase transitional properties were investigated using differential scanning calorimetry (DSC, Mettler Star 821^e), with heating and cooling rates of $5^\circ C\,min^{-1}$. Texture observation was conducted on a Leica DMLP polarising optical microscope equipped with a Leitz 350 microscope heating stage. Glass coated with Teflon was used to make planar alignment cell. X-ray diffraction (XRD) was carried out with a Bruker Avance D8 X-ray diffractometer.

3. Results and discussion

Phase behaviours

The phase behaviours of **C16.*n*.C16** were investigated by polarized optical microscopy (POM) and DSC. The dimers with shorter spacer ($n=3$, 5, 6) were found to exhibit focal conic fan-shaped textures in both heating and cooling runs, indicating enantiotropic smectic behaviours, whereas **C16.10.C16** with the longest spacer is non-mesomorphic. However, the optical properties of the dimers with odd and even spacer were noticeably different. In **C16.3.C16** and **C16.5.C16**, the extinguish brushes are parallel/perpendicular to the polariser, indicating that the director is along the layer normal, whereas in **C16.6.C16** the extinguish brushes are tilted with respect to the polariser (Figure 1(a)), indicating that the director makes a tilt angle to the layer normal. Moreover, under the planar alignment condition, **C16.5.C16** behaves as a uniaxial, birefringent plate of crystal with the optical axis in the plane of substrate; the director is perpendicular to the layer plane (Figure 1(b)), which can further confirm the assignment of smectic A (SmA) phase. Unfortunately, due to the high phase transition temperature, alignment of the other samples could not be obtained. However, based on these results, it is clear that **C16.3.C16** and **C16.5.C16** exhibit SmA phase, whereas **C16.6.C16** exhibits a smectic C (SmC) phase.

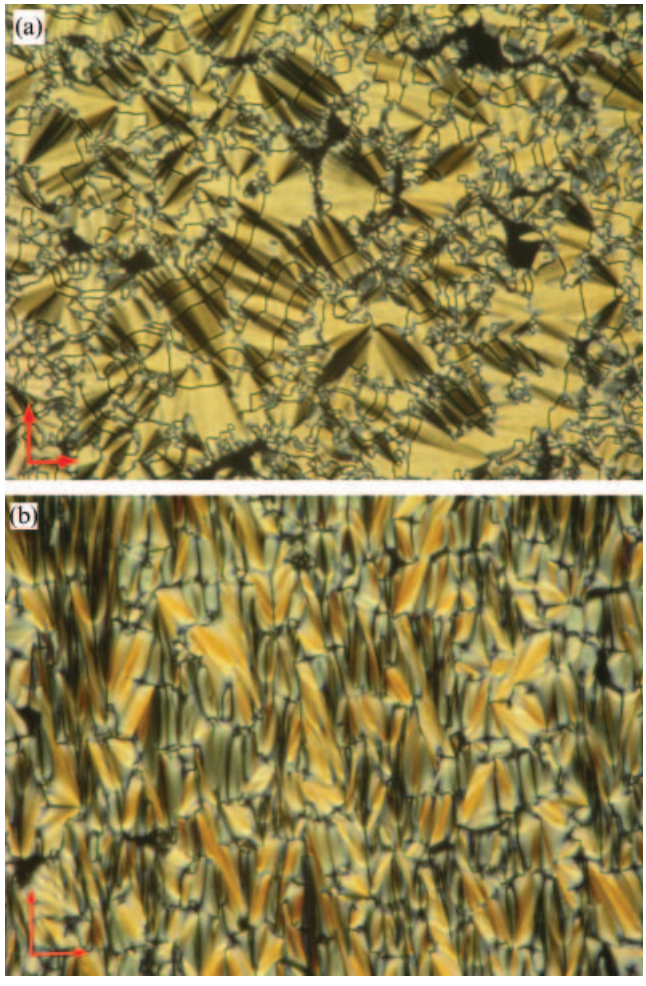

Figure 1. (a) The fan-shaped texture of **C16.6.C16** at 218°C ($\times 200$). (b) Planar alignment focal conic fan-shaped texture of **C16.5.C16** at 218°C ($\times 200$). The red arrows indicate the direction of the polarisers.

Table 1. Phase behaviours of **C16.*n*.C16** (Cr, Sm and I indicate the crystalline state, smectic phase and isotropic liquid, respectively).

Compound	Cr_1	T /°C	Cr_2	T /°C (ΔH /kJ mol^{-1})	Sm	T /°C (ΔH /kJ mol^{-1})	I
C16.3.C16	•	133.6	•	242.1 (65.91)	•	254.8 (5.25)	•
C16.5.C16	•	123.3	•	232.0 (71.84)	•	234.8 (8.86)	•
C16.6.C16	•	206.1	•	223.6 (51.93)	•	246.0 (26.69)	•
N10	•	223.3	•	237.5 (68.68)	•	301.9 (—)[a]	—

[a]**N10** degrades near the isotropic transition.

Apart from the confirmed smectic phases, DSC analysis of **C16.*n*.C16** also revealed a Cr–Cr (Cr=crystal) transition during heating. Table 1 summarises the phase transition temperatures and the associated enthalpy changes of **C16.*n*.C16**. The odd–even effect, which is a characteristic of liquid crystal dimers, is evidenced by the fact that the clearing point of **C16.6.C16** is 11.2°C higher than that of **C16.5.C16** and the enthalpy changes of clearing transition of even members are several times larger than those of the odd ones.

It is important to note that on elongating the spacer from three carbon atoms to five, the mesophase is destabilised, and from six to ten, the mesophase disappears, indicating that thermal stability of the smectic phase of **C16.*n*.C16** decrease with the spacer length. This phase behaviour is in contrast to that of the **N*n*** series, for which the clearing points increased and the mesophase ranges broadened with the length of spacer (*13*). This phenomenon is in accordance with results in the literature (*11, 15, 18*), and is understandable if one notes that the spacers act as the only flexible liquid phase in an intercalated structure with a strongly polar group.

Mesophase structure

In order to reveal the molecular packing in its mesophase, variable temperature XRD was performed on **C16.*n*.C16**. Characteristic patterns of disordered smectic phase were observed for **C16.*n*.C16** (as shown in Figure 2 for **C16.5.C16** and **C16.6.C16**), which contain sharp peaks in the low-angle region implying the formation of a layered structure, and a broad halo in the wide-angle region centred at a spacing of 4.6 Å, indicating liquid-like arrangement of the molecules within the layers. The presence of higher harmonics of the signal related to the layer spacing implies that the smectic layers should have a sharp boundary.

Data for layer spacings (d), calculated molecular lengths (l) and d/l ratios of **C16.*n*.C16** in their mesophases are collected in Table 2. It should be noted that by considering the spacer to exist in its all-*trans* conformation, an odd-membered dimer has a bent shape in which the mesogenic units are inclined to each other, whereas an even-membered dimer has a zigzag shape in which the mesogenic units are antiparallel, so the calculated molecular lengths of the odd-membered dimers are much shorter than those of the even-membered ones (Table 2). The layer spacings of **C16.3.C16** and **C16.5.C16** are almost equal to their corresponding molecular lengths, whereas the layer spacing of **C16.6.C16** is measured to be much smaller than the estimated molecular length, and the d/l ratio is about 0.68. Thus, the cone angle was calculated to be about 47°, which agrees well with the results from POM.

So, it is reasonable to think that in both of the two cases, the molecules are arranged into a monolayer structure, in which terminal chains, mesogenic units and flexible alkoxy spacers are separated into three regions. However, for the dimers with odd spacer, the bent-shaped conformation is formed, so the molecular long axis is along the layer normal, termed SmA phase (as shown in Figure 3(a) for the anti-ferroelectric polar order, which will be discussed below). However, for those dimers with even spacer, due to the straight shape, the molecular long axis is tilted with respect to the layer normal, so a SmC phase is assigned (Figure 3(b)). Furthermore, the proposed molecular packing models were confirmed by the different behaviours of the second-order harmonics in XRD patterns. As shown in Figure 2(a) for **C16.5.C16**, the second-order harmonic is very weak, almost negligible; however, in Figure 2(b) for **C16.6.C16**, it is much stronger. The extinction of the second-order reflection of **C16.5.C16** suggests that the half-layer should have different symmetry, which is in accordance with our model where the two mesogenic units are tilted in the opposite direction for the dimers with odd spacer.

In addition, SmA phases of **C16.3.C16** and **C16.5.C16** with the bent-shaped molecular conformation are supposed to have polar order within the layers, and depending on direction of the polar order in the adjacent layers, either the polar direction can be parallel, which is designated as ferroelectric (FE,

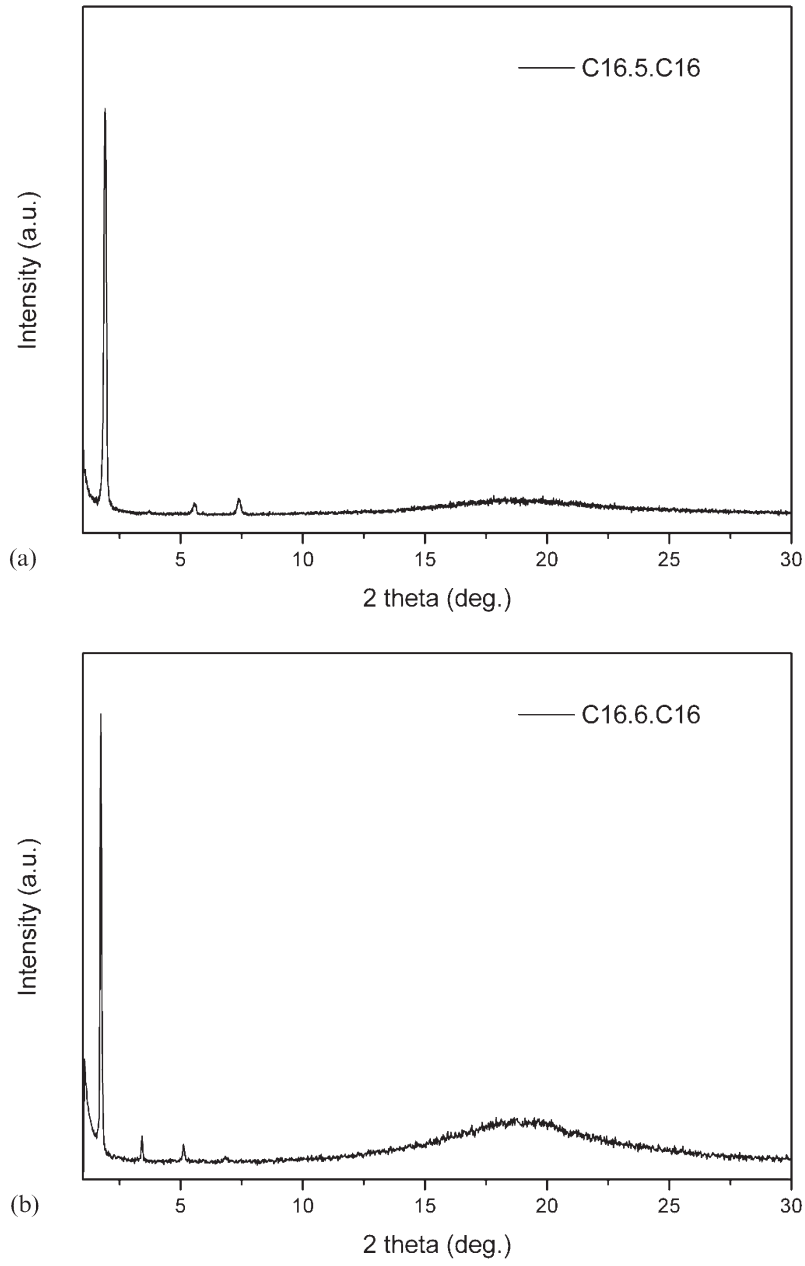

Figure 2. XRD patterns of (a) **C16.5.C16** and (b) **C16.6.C16** in their smectic phase.

not shown), or antiparallel, designated as anti-ferroelectric (AF, as shown in Figure 3(a)). Unfortunately, due to the high phase transition temperature, it is hard to prove.

Hydrogen bonding

In our previous work, we have demonstrated that the hydrogen bonding involved in these hydrazide derivatives was mainly intermolecular (*19*). As the

Table 2. Summary of X-ray diffraction results of **C16.*n*.C16** in their smectic phase.

Compound	Molecular length[a] (*l*) /Å	*T* /°C	Layer spacing (*d*) /Å	*d*/*l*
C16.3.C16	46.0	226	46.3	1.01
C16.5.C16	46.6	221	46.1	0.99
C16.6.C16	75.0	215	50.9	0.68

[a]Geometry optimisation was carried out with Austin Model 1.

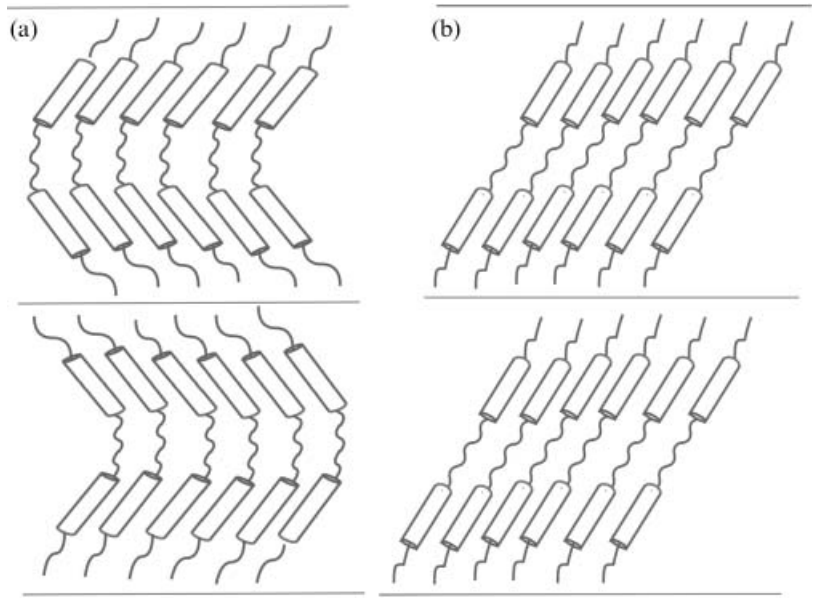

Figure 3. Sketches of monolayer structures of (a) anti-ferroelectric smectic A phase and (b) smectic C phase formed by the dimers.

mesogenic units are the same as their corresponding monomers, intermolecular hydrogen bonding was expected in these symmetric dimers. To evaluate the effect of hydrogen bonding on molecular arrangements in these mesophases, temperature dependent FT-IR spectra of **N10** (the phase transition temperatures of **N10** are shown in Table 1) and **C16.5.C16** were measured. Figures 4(a)–4(b) show the N–H vibration and amide I bands of **N10** at different temperatures. It can be seen that only hydrogen-bonded N–H (3210 cm^{-1}), strong hydrogen-bonded C=O stretching vibration bands (1592

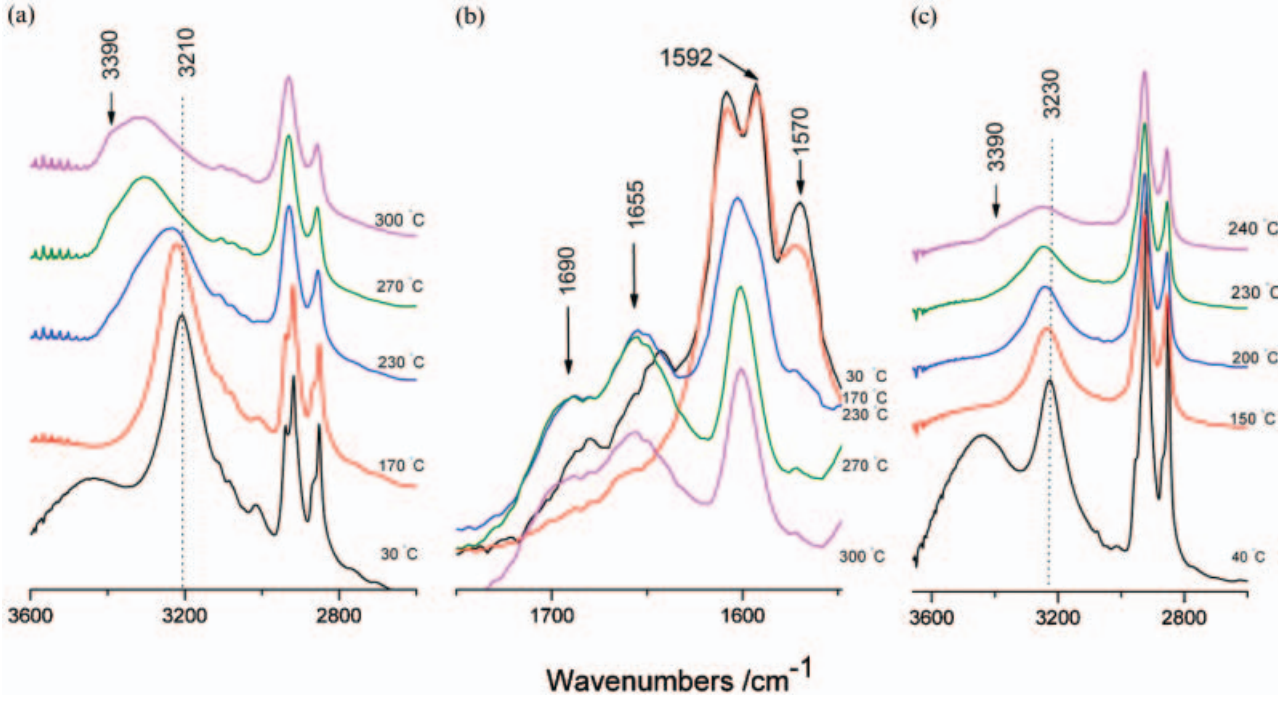

Figure 4. FT-IR spectra of **N10** in the ranges (a) 3600–2700 cm^{-1} and (b) 1800–1500 cm^{-1}, and (c) of **C16.5.C16** in the range 3600–2700 cm^{-1} at different temperatures. (The broad absorption around 3440 cm^{-1} at 30°C in both (a) and (c) was assigned to ν_{O-H} of H_2O included in the system, and which disappeared at about 100°C on heating)

and 1570 cm^{-1}) were observed at 1592 and 1570 cm^{-1}, and no "free" (non-bonded) N–H (3390 cm^{-1}) or C=O (1690 cm^{-1}) stretching vibration bands were detected at room temperature, which indicates that almost all the N–H groups are associated with the C=O groups via N–H···O=C hydrogen bonding in the crystalline phase.

Upon heating, the ν_{N-H} band became weaker and shifted toward higher frequencies continuously in Cr_1 and Cr_2 states, and then exhibited a sudden increase by about 80 cm^{-1} at the Cr–Sm transition (Figure 5). The ν_{N-H} band appears at around 3310 cm^{-1}, as well as a shoulder at 3390 cm^{-1} (free N–H) in the smectic phase (Figure 4(a), 270°C). These changes are accompanied by a shift of amide I bands from 1592 and 1570 cm^{-1} to 1690 and 1655 cm^{-1}, respectively (Figure 4(b)). The strong absorptions at 3310 cm^{-1} of N–H group and 1640 cm^{-1} of C=O group, and comparatively weak absorption at 3390 cm^{-1} (N–H) and 1690 cm^{-1} (C=O) (Figures 4(a)–4(b) at 270°C), strongly indicate that the hydrogen bonding still exists in the smectic phase, though it has become much weaker.

Similar conclusion can be drawn for **C16.5.C16**. As shown in Figure 4(c), strong absorption of N–H appeared at 3230 cm^{-1}, and no free N–H (3390 cm^{-1}) appeared, indicating that almost all N–H and C=O groups are hydrogen bonded at room temperature. Upon heating, although a sharp increase by about 20 cm^{-1} occurred during the transition from crystal state to smectic phase, the strong absorption at 3255 cm^{-1} and a weak shoulder at 3390 cm^{-1} clearly indicated that N–H and C=O groups are still associated in the smectic phase and even the isotropic state of **C16.5.C16**. Thus, it can be concluded that intermolecualar hydrogen bonding still exists in the smectic phases, though it is much weaker compared to that in their corresponding crystalline phases.

Substitution effect on the mesophase

It should be emphasized that nature of the terminal substitute has a profound influence on the liquid crystalline properties of these symmetric hydrazide dimers. Compounds **N*n*** with terminal nitro substituents exhibited an intercalated smectic phase (*13*), **C16.*n*.C16** with the long terminal alkoxy chains showed monolayer smectic phases, whereas **M6** (1,6-bis[*N*-(4-methylbenzoyl)-*N*′-(benzoyl-4′-oxy)hydrazine]hexane, Scheme 1) with methyl groups, is non-mesomorphic (*13*). The difference in phase behaviour of these compounds can be explained by the fact that the driving forces for intercalated and monolayer structures are different. Generally speaking, occurrence of the monolayer smectic phase might be the result of microphase separation between the incompatible segments, whereas the intercalated smectic phase is driven by

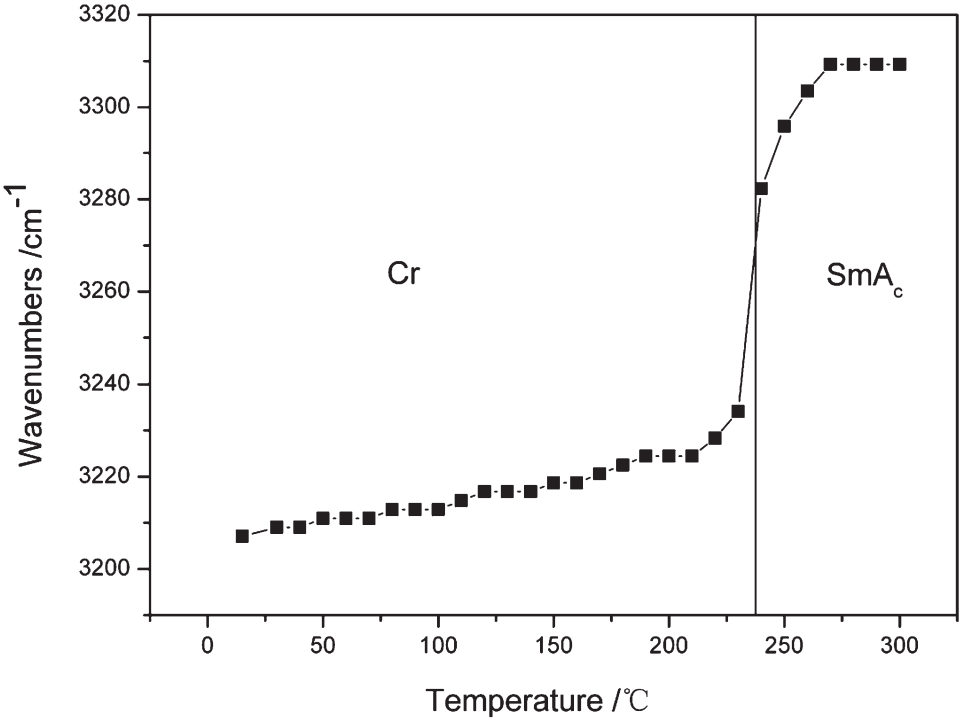

Figure 5. The temperature dependent N–H stretching vibrations of **N10** (Cr and SmA_c indicate the crystalline state and intercalated smectic A phase, respectively).

the special interactions between mesogenic units. So **N*n*** series with intermolecular hydrogen bonding between the hydrazide groups, as well as the synergistic dipole–dipole interaction arising from the strongly polar substituents ($-NO_2$), exhibit intercalated smectic phase, **C16.*n*.C16** series with enhanced microphase segregation between the long terminal chains and the rigid mesogenic cores show the monolayer smectic phases, whereas **M6** without either dipole–dipole interaction or enhanced micro-segregation, are non-mesomorphic. It should be noted that although hydrogen bonding still exists in the monolayer smectic phase of **C16.*n*.C16** (as proved by FT-IR spectra in the hydrogen bonding section), microphase segregation is in favour of the monolayer smectic structure, preventing the formation of an intercalated structure.

4. Conclusions

A series of symmetric dimers containing hydrazide groups and long terminal chains have been synthesised. It was found that the dimers with shorter spacer (**C16.*n*.C16**, $n=3$, 5, 6) exhibit enantiotropic smectic phases, whereas **C16.10.C16** with the longest spacer is non-mesomorphic. Moreover, it was confirmed that the odd-membered dimers (**C16.3.C16** and **C16.5.C16**) exhibit monolayer SmA phases, whereas the even membered dimer (**C16.6.C16**) exhibits a monolayer SmC phase, where the incompatibility between the terminal chains, mesogenic groups and the spacers is thought to be the driving force for both of these monolayer smectic structures.

Acknowledgements

This work was supported by Program for New Century Excellent Talents in Universities of China Ministry of Education, Special Foundation for PhD Program in Universities of China (MOE, Project No. 20050183057), Project 985-Automotive Engineering of Jilin University, and the State Scholarship Fund from the China Scholarship Council.

References

(1) Imrie C.T.; Luckhurst G.R. In *Handbook of Liquid Crystals*, Vol. 2B; Demus D., Goodby J.W., Gray G.W., Spiess H.W., Vill V. (Eds), Wiley-VCH: Weinheim, 1998, pp. 801–833.
(2) Imrie C.T. *Struct. Bond.* **1999,** *95*, 149–192.
(3) Imrie C.T.; Henderson P.A. *Curr. Opin. Colloid Interface Sci.* **2002,** *7*, 298–311.
(4) Imrie C.T.; Henderson P.A. *Chem. Soc. Rev.* **2007,** *36*, 2096–2124.
(5) Vorländer D. *Z. Phys. Chem.* **1927,** *126*, 449–472.
(6) Griffin A.C.; Britt T.R. *J. Am. Chem. Soc.* **1981,** *103*, 4957–4959.
(7) Rault J.; Liebert L.; Strzelecki L. *Bull. Soc. Chem. Fr.* , 1175.
(8) Huh S.M.; Jin J.I.; Achard M.F.; Hardouin F. *Liq. Cryst.* **1998,** *25*, 285–293.
(9) Jin J.I.; Kim J.S.; Yun Y.K.; Chin W.C. *Mol. Cryst. Liq. Cryst.* **1997,** *308*, 99–110.
(10) Yelamaggad C.V.; Prasad S.K.; Nair G.G.; Shashikala I.S.; Shankar Rao D.S.; Lobo C.V.; Chandrasekhar S. *Angew. Chem. Int. Ed.* **2004,** *43*, 3429–3432.
(11) Attard G.S.; Date R.W.; Imrie C.T.; Luckhurst G.R.; Roskilly S.J.; Seddon J.M.; Taylor L. *Liq. Cryst.* **1994,** *16*, 529–581.
(12) Le Masurier P.J.; Luckhurst G.R. *Chem. Phys. Lett.* **1998,** *287*, 435–441.
(13) Wang H.T.; Bai B.L.; Zhang P.; Long B.H.; Tian W.J.; Li M. *Liq. Cryst.* **2006,** *33*, 445–450.
(14) Sepelj M.; Lesac A.; Baumeister U.; Diele S.; Bruce D.W.; Hamersak Z. *Chem. Mater.* **2006,** *18*, 2050–2058.
(15) Date R.W.; Imrie C.T.; Luckhurst G.R.; Seddon J.M. *Liq. Cryst.* **1992,** *12*, 203–238.
(16) Li M.; Guo C.W.; Wu Y.Q. *Liq. Cryst.* **2002,** *29*, 1031–1037.
(17) Bai B.L.; Li M.; Pang D.M.; Wu Y.Q.; Zhang H.H. *Liq. Cryst.* **2005,** *32*, 755–761.
(18) Blatch A.E.; Luckhurst G.R. *Liq. Cryst.* **2000,** *27*, 775–778.
(19) Pang D.M.; Wang H.T.; Li M. *Tetrahedron* **2005,** *61*, 6108–6114.